Available on CMS information server

CMS NOTE 2005/xxx

The Compact Muon Solenoid Experiment

CMS Note

Mailing address: CMS CERN, CH-1211 GENEVA 23, Switzerland

29 Nov. 2005

Measurement of Missing Transverse Energy With the CMS Detector at the LHC

Haifeng Pi [*) a)], D. Acosta [a)], P. Avery [a)], D. Green [b)], J. Rohlf [c)], and C. Tully [d)]

a) University of Florida, Gainesville, FL 32601, USA
b) Fermi National Accelerator Laboratory, Batavia, IL 60510, USA
c) Boston University, Boston, MA 02532, USA
d) Princeton University, Princeton, NJ 08544, USA

Abstract

The performance of the Compact Muon Solenoid detector for measuring missing transverse energy is evaluated using fully simulated pp collisions at a center-of-mass energy of 14 TeV at the Large Hadron Collider. For minimum bias events without pileup, a resolution of 6.1 GeV is computed, corresponding to a stochastic contribution of $0.63\sqrt{\Sigma E_{\mathrm{T}}}\ \mathrm{GeV}^{1/2}$, where ΣE_{T} is the summed transverse energy in all calorimeter towers. When the contribution of pileup is included, the resolution degrades according to the overall deposited ΣE_{T} with the same stochastic coefficient. For QCD events with event pileup corresponding to a luminosity $\mathcal{L} = 2 \times 10^{33}\ \mathrm{cm}^{-2}\mathrm{s}^{-1}$, we compute $\sigma = [(3.8\ \mathrm{GeV})^2 + (0.97\ \mathrm{GeV}^{1/2}\sqrt{\Sigma E_{\mathrm{T}}})^2 + (0.012\Sigma E_{\mathrm{T}})^2]^{1/2}$ resulting in a resolution of 45 GeV for jet events with transverse momentum of 700 GeV/c. A sample of $\mathrm{t\bar{t}}$ events with lepton decays leading to true missing transverse energy was used to determine the azimuthal angle resolution to be 0.1 radians (0.2 radians) for a reconstructed missing transverse energy of 200 GeV (100 GeV).

[*)] Work done in partial requirement to fulfill the PhD degree.

1 Introduction

It is well known that the understanding of detector response to standard model physics from quantum chromodynamics (QCD) is a prerequisite to the search for new phenomena at the Large Hadron Collider (LHC). Beginning with UA1 [1], all major detectors at hadron colliders have been designed to cover as much solid angle as practically possible with calorimetry. This was a major consideration in the design of calorimetry for the Compact Muon Solenoid (CMS) [2]. The primary motivation is to provide as complete of a picture as possible of the event, including the presence of one or more energetic neutrinos or other weakly-interacting stable particles though apparent missing energy. Energetic particles produced in the direction of the beam pipe make it impossible to directly measure missing energy longitudinal to the beam direction, however, the transverse energy balance can be measured with an accuracy good enough to help establish a physics signature involving one or more non-interacting particles. The W boson was discovered and its mass determined to 3% with just 6 events due to the ability of UA1 to infer the presence of 40-GeV neutrinos with a resolution of a few GeV [3]. Since the time of the W discovery, measurement of missing transverse energy has been a major tool in the search for new phenomena at hadron colliders [4],[5].

Measurement of the missing transverse energy vector ($\mathbf{E}_{\mathrm{T}}^{\mathrm{miss}}$) in events at the LHC will be complicated by the presence of pileup collisions. In CMS, measurement of $\mathbf{E}_{\mathrm{T}}^{\mathrm{miss}}$ will be further degraded by the difference between photon and pion response in the calorimeters and by the bending of tracks by the 4-T magnetic field. On the other hand, the excellent cell segmentation, hermeticity, and good forward coverage of CMS will help measurement of $\mathbf{E}_{\mathrm{T}}^{\mathrm{miss}}$.

2 Calculation of Missing Transverse Energy in CMS

Readout cells in the CMS hadron calorimeter (HCAL) are arranged in a tower pattern in η, φ space, projective to the nominal interaction point. The HCAL cells have a segmentation of 0.087×0.087 in the central region ($|\eta| < 1.74$) and approximately 0.17×0.17 for $1.74 < |\eta| < 5$ [2]. Since the granularity of the electromagnetic crystal calorimeter (ECAL) [6] is much finer (0.017×0.017) than HCAL, calorimeter towers (ECAL plus HCAL) are formed by addition of signals in η, φ bins corresponding to individual HCAL cells. In total there are 4176 such towers, which when unfolded, may be represented in a familiar "lego" plot (Fig. 1) [7].

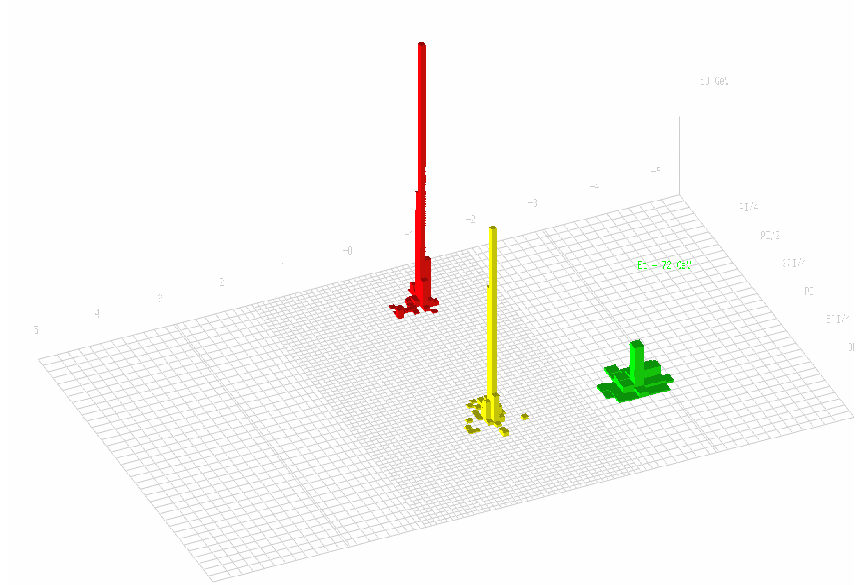

Figure 1: The η, φ tower segmentation in CMS. The towers are defined to match the granularity of the hadron calorimeter.

The missing transverse energy vector is calculated by summing individual calorimeter towers having energy E_n, polar angle θ_n and azimuthal angle φ_n:

$$\mathbf{E}_{\mathrm{T}}^{\mathrm{miss}} = -\Sigma(E_n \sin\theta_n \cos\varphi_n \hat{\mathbf{i}} + E_n \sin\theta_n \sin\varphi_n \hat{\mathbf{j}}) = E_x^{\mathrm{miss}} \hat{\mathbf{i}} + E_y^{\mathrm{miss}} \hat{\mathbf{j}} \,.$$

The towers must pass a threshold cut of $E_{\mathrm{T}} > 0.5\,\mathrm{GeV}$ in order to enter the missing transverse energy sum.

Reconstructed muons are taken into account by replacing the expected calorimeter deposit (about 4 GeV) with the reconstructed track p_{T}. Section 8 discusses further corrections to the reconstructed missing transverse energy.

3 Expected Performance

Accurate measurement missing transverse energy in individual events is a difficult experimental problem, because various detector factors are known to contribute in subtle ways. These factors include energy resolution, limited detector coverage, nonlinearity of calorimeter response, detector granularity, noninstrumented material, magnetic field and its effect on low p_{T} charged particles, quantization of detector readout, electronic noise, event pileup, and underlying event. In spite of all these detector subtleties, the $\mathbf{E}_{\mathrm{T}}^{\mathrm{miss}}$ resolution in CMS is expected to be dominated by calorimeter energy resolution.

The total scalar transverse energy (ΣE_{T}), defined as the scalar E_{T} sum of all calorimeter towers in an event, is a quantity highly associated with $E_{\mathrm{T}}^{\mathrm{miss}}$ [8]. Many properties of reconstructed missing transverse energy can be expressed as a function of ΣE_{T} because of its direct influence on the $E_{\mathrm{T}}^{\mathrm{miss}}$ resolution via stochastic effects of calorimeter showers and the process of signal collection. The missing transverse energy resolution is normally determined by fitting the width of the measured E_x^{miss} or E_y^{miss} distribution in a sample of events in which no missing transverse energy is expected [3]. In minimum bias collisions at UA1, the resolution was observed to follow the form $\sigma = 0.4\sqrt{\Sigma E_{\mathrm{T}}}\ \mathrm{GeV}^{1/2}$ where the constant 0.4 depends directly on the stochastic term $0.8\sqrt{E_{\mathrm{T}}}\ \mathrm{GeV}^{1/2}$ in the calorimeter resolution [3],[9]. The CDF experiment, which has a scintillating tile geometry similar to CMS (and a completely different magnetic field configuration compared to UA1, solenoid *vs.* dipole), observed a transverse energy resolution of $\sigma = 0.47\sqrt{\Sigma E_{\mathrm{T}}}\ \mathrm{GeV}^{1/2}$ in Run I [10]. From the UA1 and CDF results and the measured CMS calorimeter resolution stochastic term from test beam of $1.15\sqrt{E_{\mathrm{T}}}\ \mathrm{GeV}^{1/2}$ [11], one may expect a missing transverse resolution in CMS of $\sigma \approx (0.6 - 0.7)\sqrt{\Sigma E_{\mathrm{T}}}\ \mathrm{GeV}^{1/2}$ for minimum bias events with no pileup, when dominated by the shower fluctuations.

4 Event Samples

Previous studies of $E_{\mathrm{T}}^{\mathrm{miss}}$ in CMS [12] were limited by the use of less sophisticated simulation and reconstruction tools. A more advanced understanding of $E_{\mathrm{T}}^{\mathrm{miss}}$ in the CMS detector has required the large event samples available from the recent data challenge [13]. These Monte Carlo events with full-detector simulation have been used to study the $E_{\mathrm{T}}^{\mathrm{miss}}$ performance of the CMS detector and to develop correction techniques, as well as to evaluate and optimize the trigger.

The samples were generated with PYTHIA [14] using the CMS software package CMKIN 3.0.0 [15], simulated with Geant4 [16] using the CMS software package OSCAR 2.4.5 [17], and digitized with the CMS object-oriented reconstruction code ORCA 7.6.1 [18]. The signal events are combined with low-luminosity ($\mathcal{L} = 2 \times 10^{33}\ \mathrm{cm}^{-2}\mathrm{s}^{-1}$) pileup corresponding to an average of 3.4 fully inelastic collisions per 25 ns beam crossing. The following samples were used in this study: 10^6 minimum bias events, 3.2×10^6 QCD events with parton transverse momenta $0 < \hat{p}_{\mathrm{T}} < 4000\ \mathrm{GeV}/c$, 5×10^5 W+jet events, and $4 \times 10^5\ \mathrm{t\bar{t}}$ events. Details about the data samples, generation and simulation parameters, and reconstruction description can be found in ref. [19].

Event reconstruction and physics analysis was performed with ORCA 8.7.1 [18]. No additional thresholds on the calorimeter towers, beyond the $E_{\mathrm{T}} > 0.5\ \mathrm{GeV}$ already mentioned, are applied for jet reconstruction or the $E_{\mathrm{T}}^{\mathrm{miss}}$ calculation. Muons reconstructed at level-3 (offline) are included in the determination of $E_{\mathrm{T}}^{\mathrm{miss}}$. No significant difference is observed in the $E_{\mathrm{T}}^{\mathrm{miss}}$ resolution for the QCD samples between two different muon algorithms used in ORCA.

5 Performance in Soft Collisions

5.1 Minimum Bias Without Pileup

Figure 2 shows the distribution of reconstructed ΣE_{T} from a high-statistics sample of fully-simulated minimum bias events without pileup. The event simulation includes single and double diffraction. There is a minimum value of reconstructed ΣE_{T}, an offset, that is dependent on the calorimeter cell thresholds, cooresponding to an online zero-suppression, that are used to form the calorimeter towers. For this sample, the offset is 142 GeV. The average value of 194 GeV in Fig. 2 corresponds to ΣE_{T} of 52 GeV above the offset. This 52 GeV of event activity determines the size of the stochastic term in the $E_{\mathrm{T}}^{\mathrm{miss}}$ resolution for this sample. Figure 3 shows the distribution

of $E_x^{\rm miss}$. The width of this distribution is $\sigma = 6.1$ GeV in agreement with expectation of addition in quadrature of a 3.8 GeV noise term and a $0.63\sqrt{\Sigma E_{\rm T}}$ GeV$^{1/2}$ stochastic term. It is important to note that at this stage, the vector $\mathbf{E}_{\rm T}^{\rm miss} = E_x\hat{\mathbf{i}} + E_y\hat{\mathbf{j}}$ is made using towers that have been formed from ECAL cells calibrated for photons and HCAL cells calibration for hadrons, appropriate perhaps for understanding the detector response to first collisions. It is believed that making use of energy flow techniques such as the charged track corrections [20] will ultimately improve the $E_{\rm T}^{\rm miss}$ resolution.

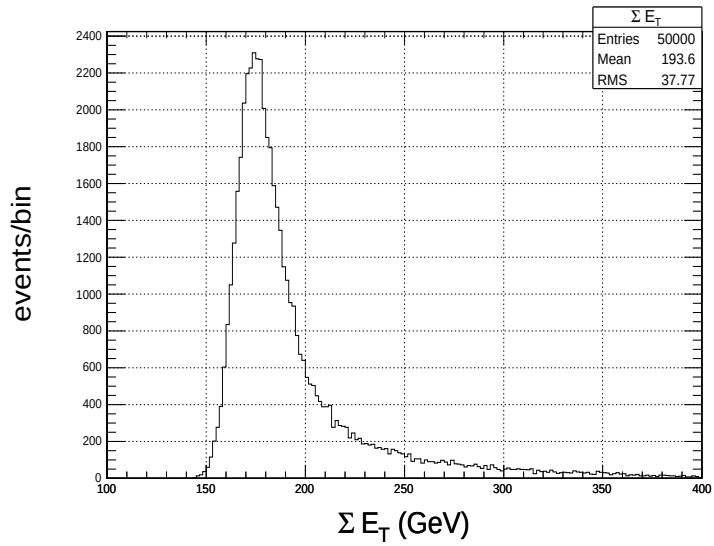

Figure 2: Distribution of $\Sigma E_{\rm T}$ for minimum bias events with no pileup. The reconstructed offset (minimum value of $\Sigma E_{\rm T}$ of 142 GeV depends on calorimeter thresholds.

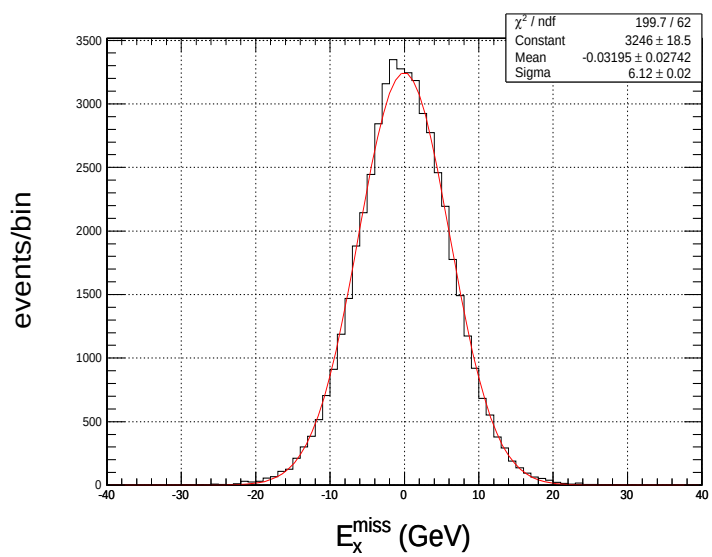

Figure 3: Distribution of $E_x^{\rm miss}$ for minimum bias events with no pileup. The resolution is 6.1 GeV is in agreement with expectations based on a stochastic term of $0.63\sqrt{\Sigma E_{\rm T}}$ GeV$^{1/2}$ and a noise contribution of 3.8 GeV.

5.2 Soft Collisions With Pileup

The addition of pileup increases the observed $\Sigma E_{\rm T}$ as shown in Fig. 4 for a sample of soft QCD collisions with $0 < \hat{p}_{\rm T} < 15$ GeV$/c$. The average value of $\Sigma E_{\rm T}$ in the sample shown in Fig. 4 is 166 GeV greater than that of the minimum bias sample without pileup (Fig. 2). The corresponding missing transverse energy resolution (Fig. 5) is 9.9 GeV. This increase from 6.1 GeV (without pileup) to 9.9 GeV (with pileup) is in agreement with expectations from a stochastic term of $0.63\sqrt{\Sigma E_{\rm T}}$ GeV$^{1/2}$. Thus, the presence of pileup does not adversely affect the $E_{\rm T}^{\rm miss}$ resolution beyond raising the overall activity ($\Sigma E_{\rm T}$) of the event.

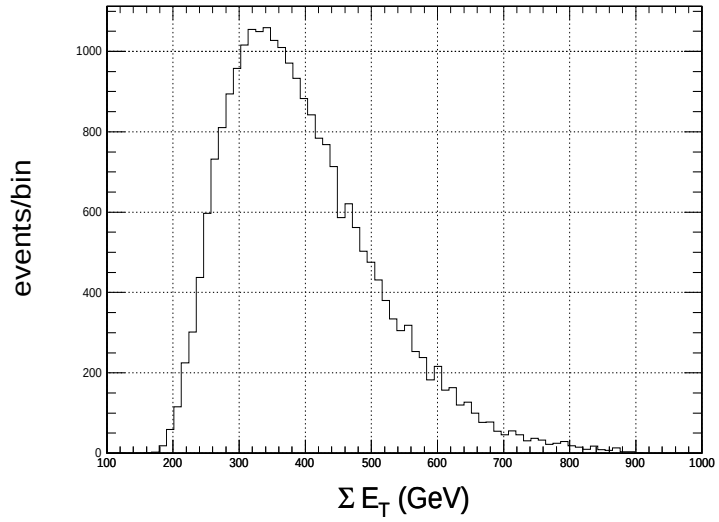

Figure 4: Distribution of ΣE_{T} for soft QCD collisions ($0 < \hat{p}_{\mathrm{T}} < 15\ \mathrm{GeV}/c$), including in-time event pileup corresponding to a luminosity of $\mathcal{L} = 2 \times 10^{33}\mathrm{cm}^{-2}\mathrm{s}^{-1}$.

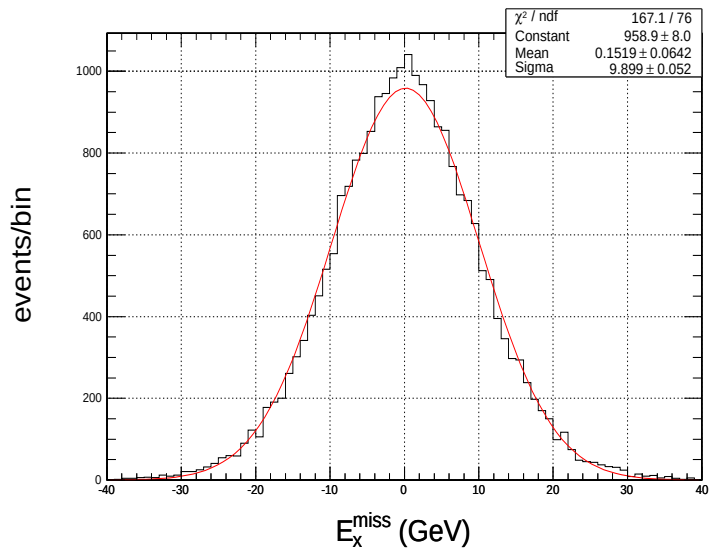

Figure 5: Distribution of E_x^{miss} for soft QCD collisions ($0 < \hat{p}_{\mathrm{T}} < 15\ \mathrm{GeV}/c$), including in-time event pileup corresponding to a luminosity of $\mathcal{L} = 2 \times 10^{33}\mathrm{cm}^{-2}\mathrm{s}^{-1}$. The resolution is 9.9 GeV.

A more detailed comparison of the reconstructed missing transverse energy resolution from minimum bias events and soft QCD events is shown in Fig. 6. The minimum bias and QCD samples of Fig. 6 both include in-time event pileup corresponding to a luminosity of $\mathcal{L} = 2 \times 10^{33}\mathrm{cm}^{-2}\mathrm{s}^{-1}$. Figure 6 shows the $E_{\mathrm{T}}^{\mathrm{miss}}$ resolution, determined from fits to reconstructed E_x^{miss} distributions like that of Fig. 5, for minimum bias events (open circles) and soft QCD events, $0 < \hat{p}_{\mathrm{T}} < 15\ \mathrm{GeV}/c$, (solid squares). The resolution as a function of ΣE_{T} has parameterized with a fit (solid curve in Fig. 5) that gives

$$\sigma = [(4.0\ \mathrm{GeV})^2 + (0.63\ \mathrm{GeV}^{1/2}\sqrt{\Sigma E_{\mathrm{T}} - 142\ \mathrm{GeV}})^2]^{1/2}.$$

The stochastic term is the same as observed in minimum bias collisions with no pileup (Fig, 3).

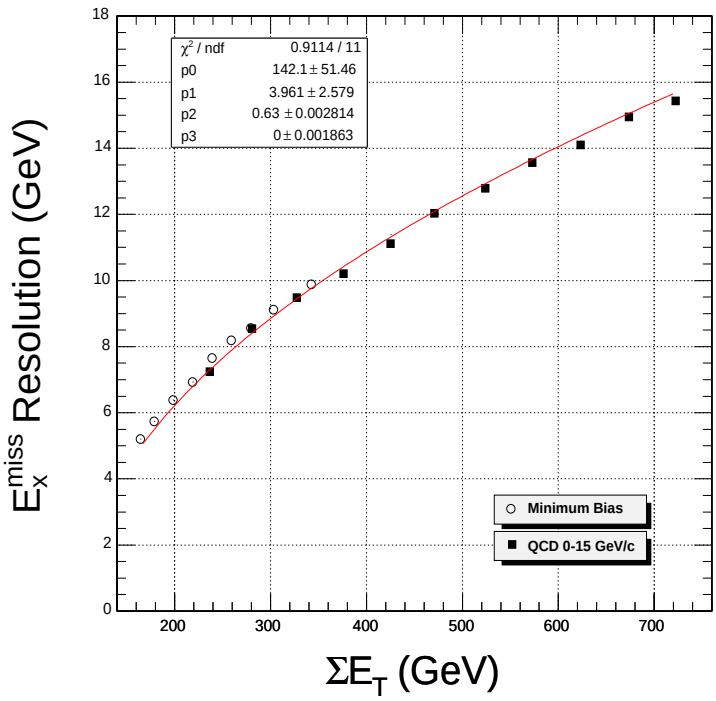

Figure 6: Missing transverse energy resolution, as determined from Gaussian fits to distributions of reconstructed $E_x^{\rm miss}$, *vs.* reconstructed $\Sigma E_{\rm T}$ for QCD soft events, $0 < \hat{p}_{\rm T} < 15$ GeV/c, (solid squares) and minimum bias events (open circles), including in-time event pileup corresponding to a luminosity of $\mathcal{L} = 2 \times 10^{33}{\rm cm}^{-2}{\rm s}^{-1}$. The resolution (curve) has been fit to $\sigma = [(4.0\ {\rm GeV})^2 + (0.63\ {\rm GeV}^{1/2}\sqrt{\Sigma E_{\rm T} - 142\ {\rm GeV}})^2]^{1/2}$.

6 Performance in Hard Collisions

6.1 Scalar Transverse Energy Sum

The distribution of reconstructed $\Sigma E_{\rm T}$ for QCD collisions with varying values of generator $\hat{p}_{\rm T}$ from 20-800 GeV are shown in Fig. 7. The samples include pileup corresponding to a luminosity of $\mathcal{L} = 2 \times 10^{33}{\rm cm}^{-2}{\rm s}^{-1}$. A relatively small $\hat{p}_{\rm T}$ interval corresponds to a wide range of $\Sigma E_{\rm T}$. Figure 8 shows the ratio of reconstructed $(\Sigma E_{\rm T})_{\rm r}$ to generated $(\Sigma E_{\rm T})_{\rm g}$ summed transverse energy *vs.* $(\Sigma E_{\rm T})_{\rm g}$. The larger value of $(\Sigma E_{\rm T})_{\rm r}$ compared to $(\Sigma E_{\rm T})_{\rm g}$ at small values of $(\Sigma E_{\rm T})_{\rm g}$ is due to a threshold-dependent offset in the reconstructed $\Sigma E_{\rm T}$ scale due to electronic noise. The ratio $(\Sigma E_{\rm T})_{\rm r}/(\Sigma E_{\rm T})_{\rm g}$ may be parameterized (curve in Fig. 7) as

$$\frac{(\Sigma E_{\rm T})_{\rm r}}{(\Sigma E_{\rm T})_{\rm g}} = 0.92 + \frac{240\ {\rm GeV}}{(\Sigma E_{\rm T})_{\rm g} - 40\ {\rm GeV}}\ .$$

Figure 9 shows the contribution of pileup to the reconstructed $(\Sigma E_{\rm T})$ *vs.* generated $(\Sigma E_{\rm T})$ in QCD events. The contribution of pileup to the reconstructed $(\Sigma E_{\rm T})$ is about 350-450 GeV. The dependence of the pileup contribution on the generated (signal) $\Sigma E_{\rm T}$ comes from various detector effects including nonlinear response, electronic noise, and the $E_{\rm T}$ threshold used in calorimeter hit reconstruction (0.5 GeV).

6.2 Missing Transverse Energy Resolution

It is well known that missing transverse energy resolution measured in high momentum-transfer events will not fit the same stochastic term as soft collisions [4]. This is due in part to fragmentation effects and contributions to the jet resolution from linear terms [21]. Figure 10 shows the $E_{\rm T}^{\rm miss}$ resolution, determined from fits to reconstructed $E_x^{\rm miss}$ distributions, for QCD hard collisions, including in-time event pileup corresponding to a luminosity of $\mathcal{L} = 2 \times 10^{33}{\rm cm}^{-2}{\rm s}^{-1}$. At low values of $\Sigma E_{\rm T}$, the resolution (Fig. 10) agrees with that determined from soft collisions (Fig. 6). The resolution as a function of $\Sigma E_{\rm T}$ has been parameterized with a fit (solid curve in Fig. 10) that gives

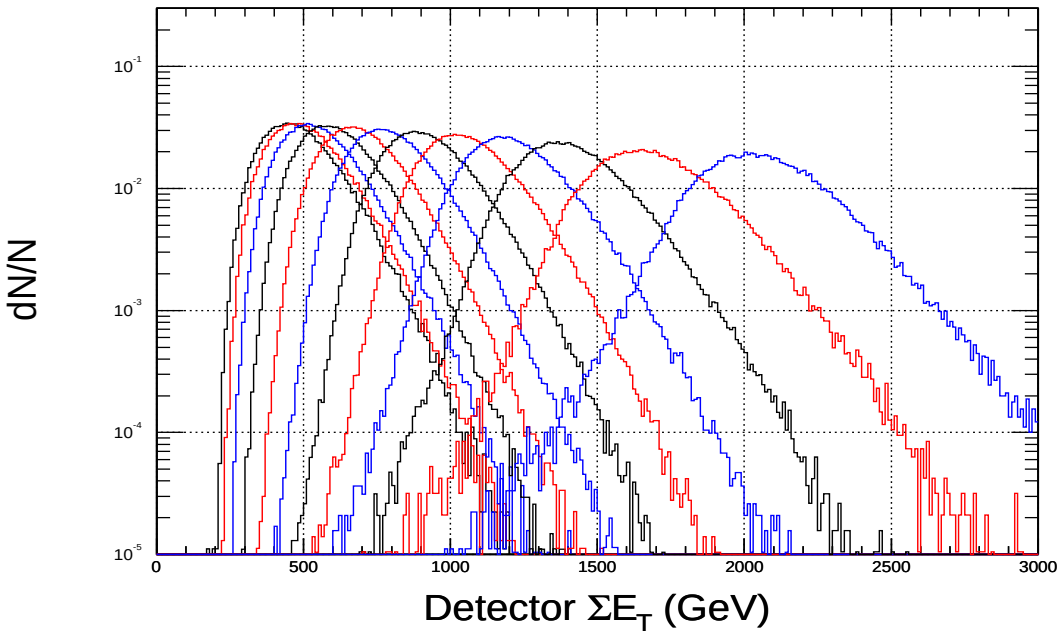

Figure 7: Reconstructed $\Sigma E_{\rm T}$ in QCD samples corresponding to $\hat{p}_{\rm T}$ ranges (from left to right) of 20-30, 30-50, 50-80, 80-120, 120-170, 170-230, 230-300, 300-380, 380-470, 470-600 and 600-800 GeV/c. The samples include pileup corresponding to a luminosity of $\mathcal{L} = 2 \times 10^{33}{\rm cm}^{-2}{\rm s}^{-1}$.

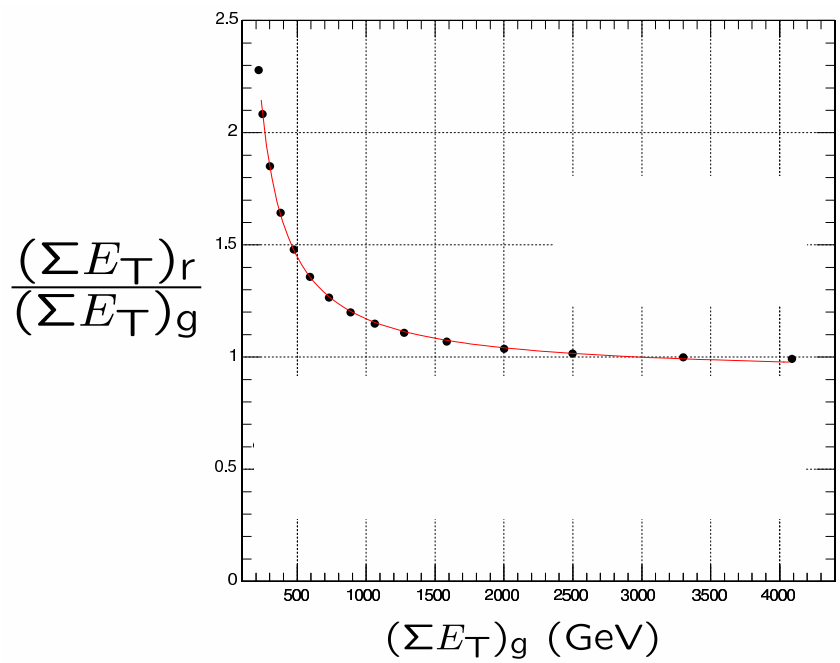

Figure 8: Ratio of reconstructed $(\Sigma E_{\rm T})_{\rm r}$ to generated $(\Sigma E_{\rm T})_{\rm g}$ summed transverse energy *vs.* $(\Sigma E_{\rm T})_{\rm g}$ from QCD events with pileup. The increase in the ratio at low values of $(\Sigma E_{\rm T})_{\rm g}$ is due to a threshold-dependent offset in $(\Sigma E_{\rm T})_{\rm r}$ caused by electronic noise. The ratio is fit (curve) to $(\Sigma E_{\rm T})_{\rm r}/(\Sigma E_{\rm T})_{\rm g} = 0.92 + 240\ {\rm GeV}/[(\Sigma E_{\rm T})_{\rm g} - 40\ {\rm GeV}]$.

$$\sigma = [(3.8\ {\rm GeV})^2 + (0.97\ {\rm GeV}^{1/2}\sqrt{\Sigma E_{\rm T} - 350\ {\rm GeV}})^2 + \ [0.012(\Sigma E_{\rm T} - 350\ {\rm GeV})]^2]^{1/2}\ .$$

The large QCD cross section at the LHC will allow us to directly measure distributions of $E_x^{\rm miss}$ and $E_y^{\rm miss}$ both with and without pileup in order to directly determine the missing transverse energy resolution under operating

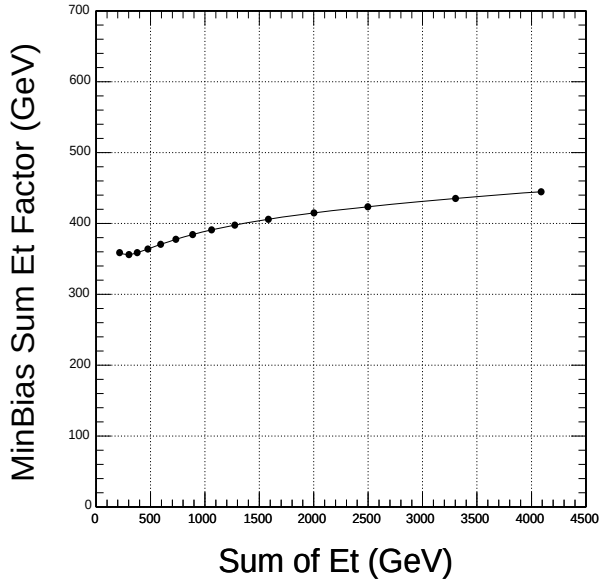

Figure 9: Contribution of pileup to reconstructed ΣE_{T} as a function of generated ΣE_{T}. The dependence on generated ΣE_{T} is due to detector effects.

conditions.

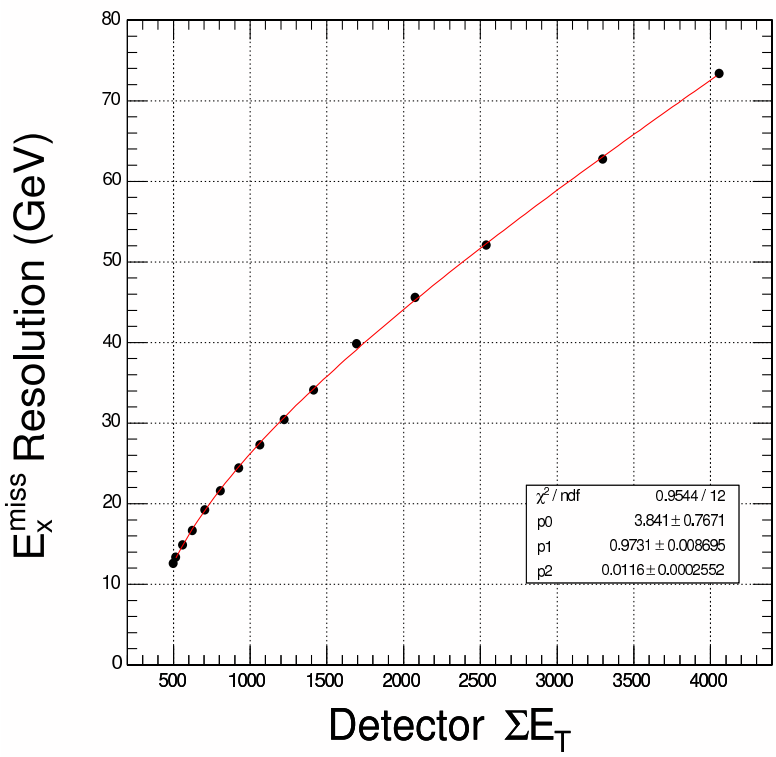

Figure 10: Missing transverse energy resolution *vs.* ΣE_{T} for QCD hard collisions, including in-time event pileup corresponding to a luminosity of $\mathcal{L} = 2 \times 10^{33} \mathrm{cm}^{-2}\mathrm{s}^{-1}$. The resolution (curve) has been fit to $\sigma = [(3.8\ \mathrm{GeV})^2 + (0.97\ \mathrm{GeV}^{1/2}\sqrt{\Sigma E_{\mathrm{T}} - 350\ \mathrm{GeV}})^2 +\ [0.012(\Sigma E_{\mathrm{T}} - 350\ \mathrm{GeV})]^2]^{1/2}$

6.3 Reconstructed Missing Transverse Energy

Reconstructed $E_{\mathrm{T}}^{\mathrm{miss}}$ in QCD events is directly related to the $E_{\mathrm{T}}^{\mathrm{miss}}$ resolution [4]. The observed $E_{\mathrm{T}}^{\mathrm{miss}}$ distribution, by its construction, has a one-sided tail. A small $\hat{p}_{\mathrm{T}}$ interval can create a wide spectrum of $E_{\mathrm{T}}^{\mathrm{miss}}$ at both generator and detector level. The reconstructed $E_{\mathrm{T}}^{\mathrm{miss}}$ for different intervals of parton-level generator $\hat{p}_{\mathrm{T}}$ are shown in Fig. 11. The samples include pileup corresponding to a luminosity of $\mathcal{L} = 2 \times 10^{33}\mathrm{cm}^{-2}\mathrm{s}^{-1}$. The distributions for each $\hat{p}_{\mathrm{T}}$ range are normalized by production cross section. The integrated cross section of the lowest $\hat{p}_{\mathrm{T}}$ interval of 20-30 GeV/c (0.8 mb) is more than 6 orders of magnitude higher than the $\hat{p}_{\mathrm{T}}$ interval of 600-800 GeV/c (0.2 nb). Thus, the inclusive $E_{\mathrm{T}}^{\mathrm{miss}}$ spectrum is expected to be dominated by low $\hat{p}_{\mathrm{T}}$ QCD events. Events with very large reconstructed $E_{\mathrm{T}}^{\mathrm{miss}}$ ($>$ 100 GeV) can be seen for large values of generated $\hat{p}_{\mathrm{T}}$, and are due mainly to energetic neutrinos and nonidentified muons.

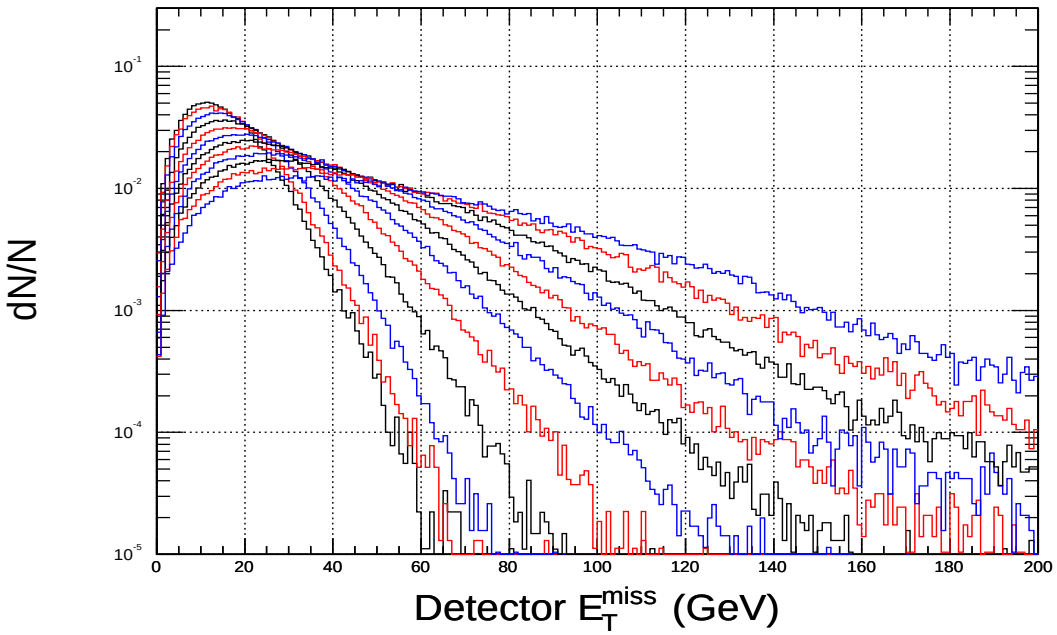

Figure 11: Reconstructed missing transverse energy spectra in QCD samples that correspond to parton-level $\hat{p}_{\mathrm{T}}$ ranges of (from left to right) 20-30, 30-50, 50-80, 80-120, 120-170, 170-230, 230-300, 300-380, 380-470, 470-600, 600-800 and 800-1000 GeV/c. The samples include pileup corresponding to a luminosity of $\mathcal{L} = 2\times10^{33}\mathrm{cm}^{-2}\mathrm{s}^{-1}$.

The reconstructed $E_{\mathrm{T}}^{\mathrm{miss}}$ in QCD events (with pileup) as a function of ΣE_{T} is shown in Fig. 12. At ΣE_{T} = 2000 GeV, which corresponds to $p_{\mathrm{T}} \approx$ 700 GeV/c jets (see Fig. 7) , an average $E_{\mathrm{T}}^{\mathrm{miss}}$ of about 60 GeV is reconstructed. This number is consistent with measurement of such jets with a resolution of $1.25\ \mathrm{GeV}^{1/2}\sqrt{E_{\mathrm{T}}}$ [22] plus a small contribution from the underlying event. A fit to the reconstructed missing transverse energy gives

$$\langle E_{\mathrm{T}}^{\mathrm{miss}} \rangle = [(5.4\ \mathrm{GeV})^2 + (1.23\ \mathrm{GeV}^{1/2}\sqrt{\Sigma E_{\mathrm{T}} - 350\ \mathrm{GeV}})^2 + \ [0.019(\Sigma E_{\mathrm{T}} - 350\ \mathrm{GeV})]^2]^{1/2}\ .$$

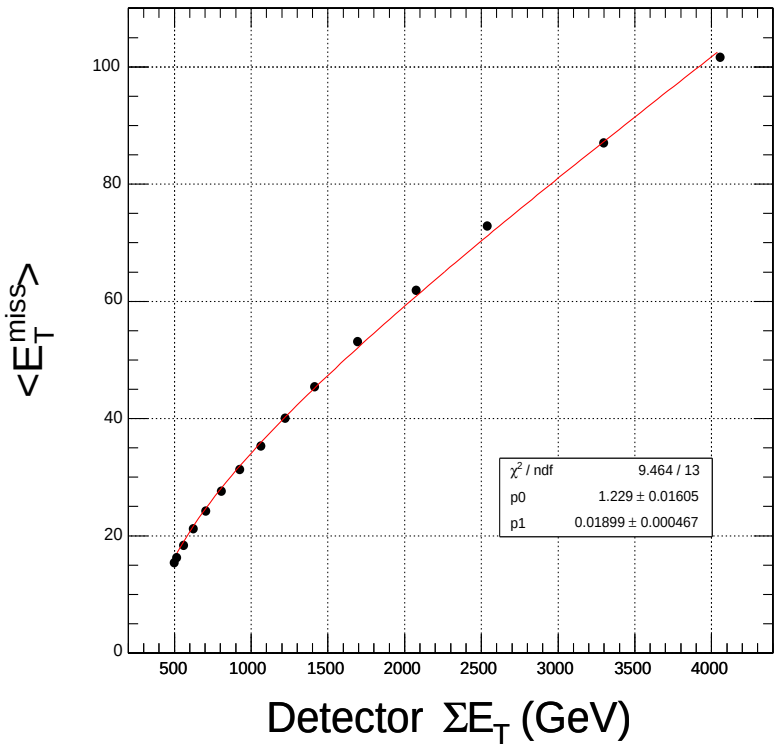

Figure 12: Average reconstructed $E_{\mathrm{T}}^{\mathrm{miss}}$ *vs.* ΣE_{T} for QCD hard collisions, including in-time event pileup corresponding to a luminosity of $\mathcal{L} = 2 \times 10^{33}\mathrm{cm}^{-2}\mathrm{s}^{-1}$. The fit (curve) corresponds to $\langle E_{\mathrm{T}}^{\mathrm{miss}} \rangle = [(5.4\ \mathrm{GeV})^2 + (1.23\ \mathrm{GeV}^{1/2}\sqrt{\Sigma E_{\mathrm{T}} - 350\ \mathrm{GeV}})^2 + [0.019(\Sigma E_{\mathrm{T}} - 350\ \mathrm{GeV})]^2]^{1/2}$.

7 Contribution of Jets and Unclustered Towers

Since jets dominate the E_{T} structure QCD events, it is interesting to investigate the contribution of jets and unclustered towers to the reconstructed missing transverse energy. Two regions are defined in an event: the jet region (defined by the jet cones) and the unclustered region (all calorimeter towers that are outside jets). The value of $E_{\mathrm{T}}^{\mathrm{miss}}$ can be calculated separately for each region. The two regions are defined by the reconstructed event at the detector level; at the generator level, particles are associated with one of the two regions based on their direction. The definition of regions is performed for every event.

Jets are reconstructed by the iterative cone (IC) algorithm implemented in ORCA with cone size of $R = 0.5$ and a minimum jet threshold of $p_{\mathrm{T}} > 20$ GeV/c [22]. The towers that do not contribute to jets are collected as unclustered towers. The jet cone size was varied to investigate the effect on the region definition and $E_{\mathrm{T}}^{\mathrm{miss}}$ quantities. We use the axis of IC jets with a $R = 0.5$ cone as input to rebuild the jets with new cone sizes of R =0.2, 0.4, 0.6 and 0.8. Fig. 13 shows the ratio of ΣE_{T} in the jet region to that in the unclustered region. as a function of reconstructed ΣE_{T} for the different cone sizes. A cone size of $R = 0.2$ contains only the core of the jet [9]. At $\Sigma E_{\mathrm{T}} = 1700$ GeV which corresponds to jets with average transverse momenta of approximately 530 GeV/c (see Fig. 7), about 3/4 of the reconstructed ΣE_{T} is inside the $R = 0.5$ jet cones. As expected, the jets play a dominant role in defining the reconstructed $E_{\mathrm{T}}^{\mathrm{miss}}$ in the event. Figure 14 shows the contributions to the missing transverse energy resolution determined separately for the jet and unclustered regions.

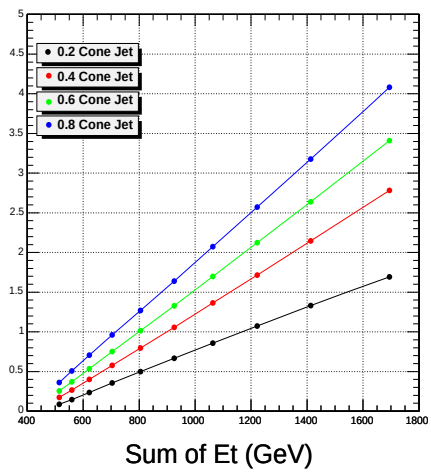

Figure 13: Ratio of reconstructed ΣE_{T} in jet region to that in the unclustered region *vs.* ΣE_{T} for jet cones of size $R = 0.2$, 0.4, 0.6, and 0.8.

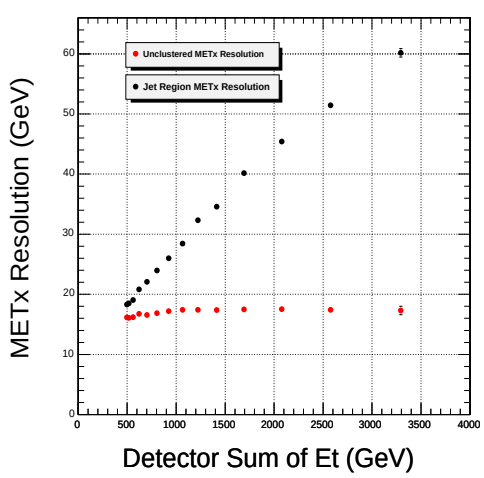

Figure 14: Contributions of deposits in the jet (upper points) and unclustered regions (lower points) to the missing transverse energy resolution. *vs.* reconstructed ΣE_{T}.

The direction (φ angle) of reconstructed missing transverse energy in the jet region is strongly correlated to that in the unclustered region indicating that the underlying event contributes to the overall balance of $E_{\rm T}^{\rm miss}$. Figure 15 shows the φ angular correlation between the missing transverse energy vector reconstructed in the jet ($\mathbf{E}_{\rm Tj}^{\rm miss}$) and the unclustered ($\mathbf{E}_{\rm Tu}^{\rm miss}$) regions for two different QCD samples, (a) $30\ {\rm GeV}/c < \hat{p}_{\rm T} < 50\ {\rm GeV}/c$ and (b) $50\ {\rm GeV}/c < \hat{p}_{\rm T} < 80\ {\rm GeV}/c$, and four different cone sizes (R = 0.2, 0.4, 0.6, and 0.8). The difference in azimuthal angle for these vectors ($\Delta\varphi$) is defined relative to a back-to-back configuration as $\Delta\varphi = \varphi_{\rm j} - \phi_{\rm u} - \pi$, where $\varphi_{\rm j}$ and $\varphi_{\rm u}$ are the azimuthal angles of the reconstructed transverse energy vectors in the jet and unclustered regions. The correlation is stronger for lower $p_{\rm T}$ jets where the importance of the underlying event for overall $E_{\rm T}^{\rm miss}$ balance is greater.

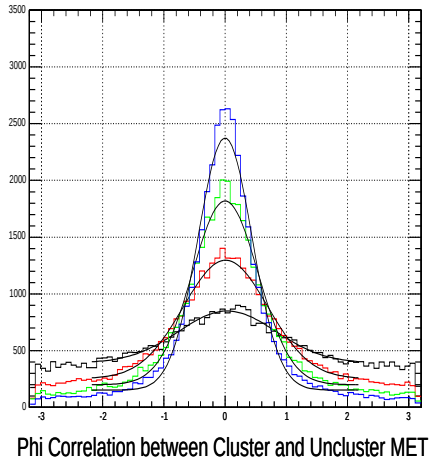

(a)

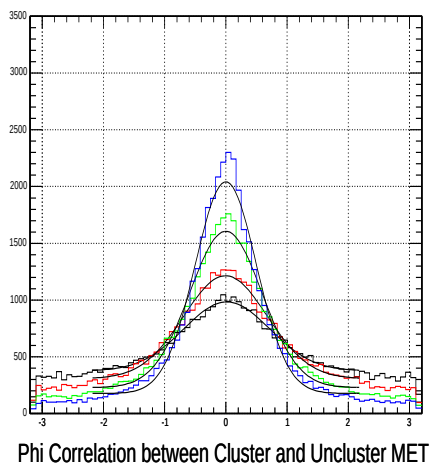

(b)

Figure 15: The φ correlation between the missing transverse energy vectors reconstructed in the jet and unclustered regions for QCD samples with (a) $\hat{p_{\rm T}}$ of 30-50 and (b) 50-80 GeV for four cone radii R =0.2, 0.4, 0.6 and 0.8. The peak shows that the vectors $\mathbf{E}_{\rm Tj}^{\rm miss}$ and $\mathbf{E}_{\rm Tu}^{\rm miss}$ are back-to-back.

Fro QCD events, it is expected that the direction of reconstructed missing transverse energy be opposite in φ to that of the most energetic jet. Fig. 16 shows the φ difference between the highest $E_{\rm T}$ jet and $\mathbf{E}_{\rm T}^{\rm miss}$.

As an additional check of detector $\mathbf{E}_{\rm T}^{\rm miss}$ performance, one may look at the resolution in a direction orthogonal to the jet axis. By choosing this direction, the observed resolution is independent of the reconstructed jet resolution, but rather is dominated by the underlying event and pileup activity. This distribution is shown in Fig. 17 *vs.* reconstructed $\Sigma E_{\rm T}$. The result may be fit to the form

$$\sigma = [(9.9\ {\rm GeV})^2 + (0.48\ {\rm GeV}^{1/2}\sqrt{\Sigma E_{\rm T} - 350\ {\rm GeV}})^2]^{1/2}\ .$$

As expected, the resolution is comparable to that observed in soft collisions (Fig. 6).

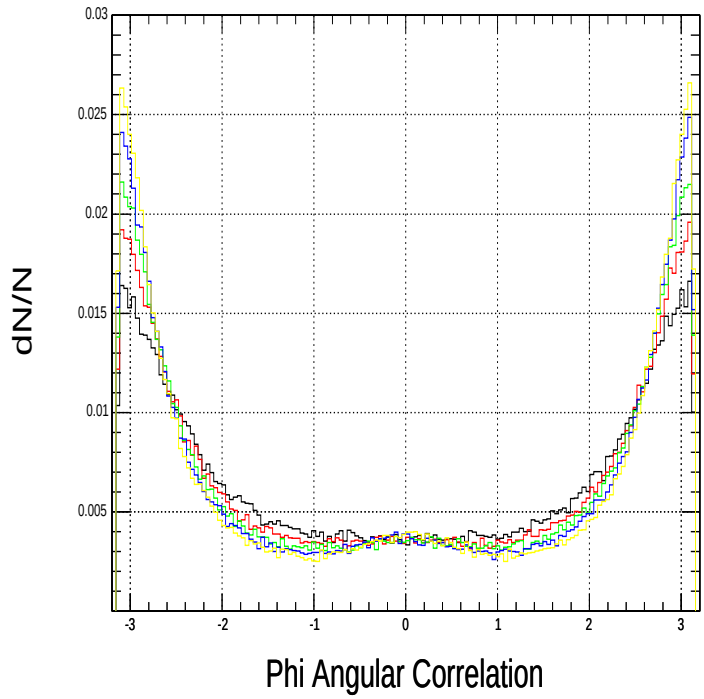

Figure 16: The φ separation between the direction of the highest E_{T} jet and the reconstructed vector $\mathbf{E}_{\mathrm{T}}^{\mathrm{miss}}$. Five $\hat{p_{\mathrm{T}}}$ QCD samples are plotted: 50-80 GeV/c (black), 80-120 GeV/c (red), 120-170 GeV/c (green), 170-230 GeV/c (blue) and 230-300 GeV/c (yellow) GeV/c.

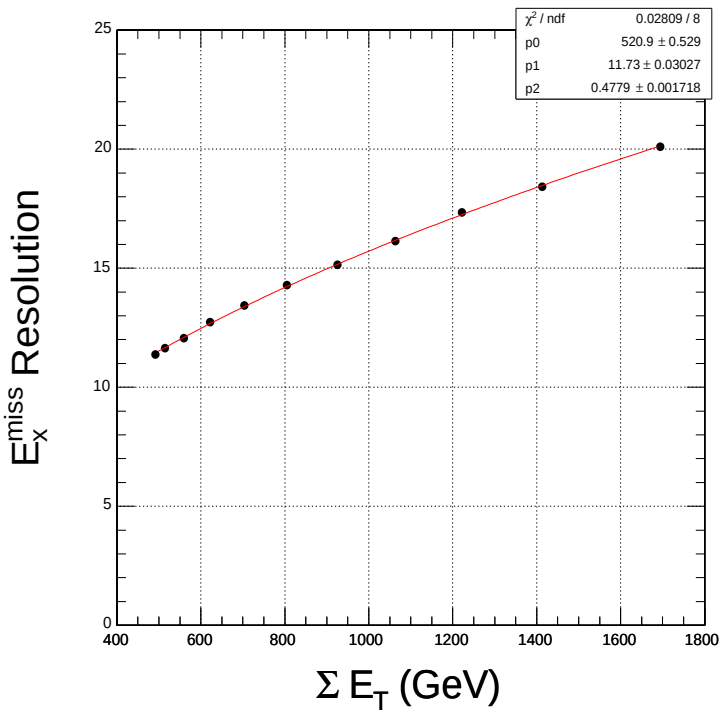

Figure 17: Missing transverse energy resolution in a direction orthogonal to the jet axis *vs.* ΣE_{T} of the entire event. The resolution is comparable to that observed in soft collisions (Fig 6). A fit (curve) gives $\sigma = [(9.9\ \mathrm{GeV})^2 + (0.48\ \mathrm{GeV}^{1/2}\sqrt{\Sigma E_{\mathrm{T}} - 350\ \mathrm{GeV}})^2]^{1/2}$

8 Corrections to $\mathbf{E}_{\mathrm{T}}^{\mathrm{miss}}$

Earlier studies [23] show that using calibrated jet energy scale can restore the average missing transverse energy scale in processes containing genuine $E_{\mathrm{T}}^{\mathrm{miss}}$, but similar methods do not significantly reduce the fake reconstructed $E_{\mathrm{T}}^{\mathrm{miss}}$ QCD events, which mainly comes from stochastic effect of calorimeter jet energy response. Samples of $\mathrm{t\bar{t}}$ and W+jet events were used to investigate the effect of jet corrections on the missing transverse energy resolution. The inclusive jet $p_{|rmT}$ spectra are shown in Fig. 18.

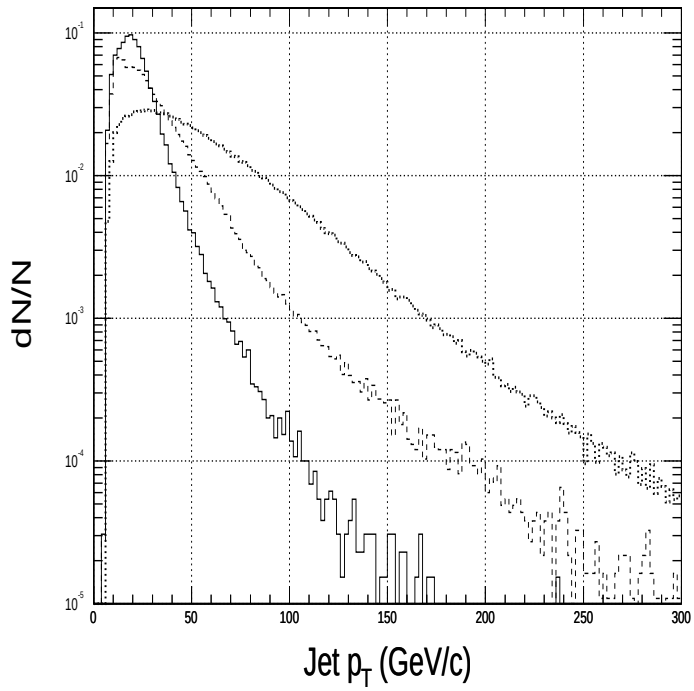

Figure 18: Inclusive jet p_{T} spectrum from QCD (solid line), $\mathrm{t\bar{t}}$ (dotted line) and W+jet with W p_T between 40 and 300 GeV (dash line).

Samples of $\mathrm{t\bar{t}}$ and W+jet with leptonic decays were used to investigate reconstruction of events which contain a true $E_{\mathrm{T}}^{\mathrm{miss}}$. Cuts on the lepton transverse momentum ($p_{\mathrm{T}} > 20$ GeV) and pseudorapidity ($|\eta| < 3.0$ for electrons and $|\eta| < 2.4$ for muons) were implemented during detector reconstruction. Jets are reconstructed using the iterative cone algorithm with a cone size $R = 0.5$, seed threshold $E_{\mathrm{T}} = 1.0$ GeV, minimum jet threshold $E_{\mathrm{T}} = 15$ GeV, and calorimeter tower threshold $E_{\mathrm{T}} = 0.5$ GeV,

Figure 19 shows the reconstructed $E_{\mathrm{T}}^{\mathrm{miss}}$ and ΣE_{T} spectrum in $\mathrm{t\bar{t}}$ and W+jet events. The $\mathrm{t\bar{t}}$ are plotted separately for the case where leptonic decay of a W is forced at the generator level. Figure 20 shows the uncorrected reconstructed jet p_{T} *vs.* generated jet p_{T} for QCD, $\mathrm{t\bar{t}}$ and W+jet events. In basing the jet corrections on QCD events, which is done in order to suppress fake E_{T}^{miss} from badly reconstructed jets, we introduce a p_{T}-dependent bias into the $\mathrm{t\bar{t}}$ and W+jet samples due to their different parton composition. A correction is then made to $\mathbf{E}_{\mathrm{T}}^{\mathrm{miss}}$ by replacing reconstructed raw jets with Monte Carlo corrected jets [22]. The main purpose of the correction, which restores the average recontructed jet E_{T} in a cone to the average generated E_{T} in the cone is to account for the nolinearity of the calorimetry. The correction factors are claculated as a function of jet p_{T} and η with QCD events Figure 21 shows the missing transverse energy resolution before and after jet corrections for (a) $\mathrm{t\bar{t}}$ events *vs.* reconstructed $E_{\mathrm{T}}^{\mathrm{miss}}$ and and (b) W+jet events *vs.* W p_{T}. Figure 22 shows the error in the reconstructed missing transverse energy scale before and after jet corrections for (a) $\mathrm{t\bar{t}}$ events *vs.* reconstructed $E_{\mathrm{T}}^{\mathrm{miss}}$ and (b) W+jet events *vs.* W p_{T}.

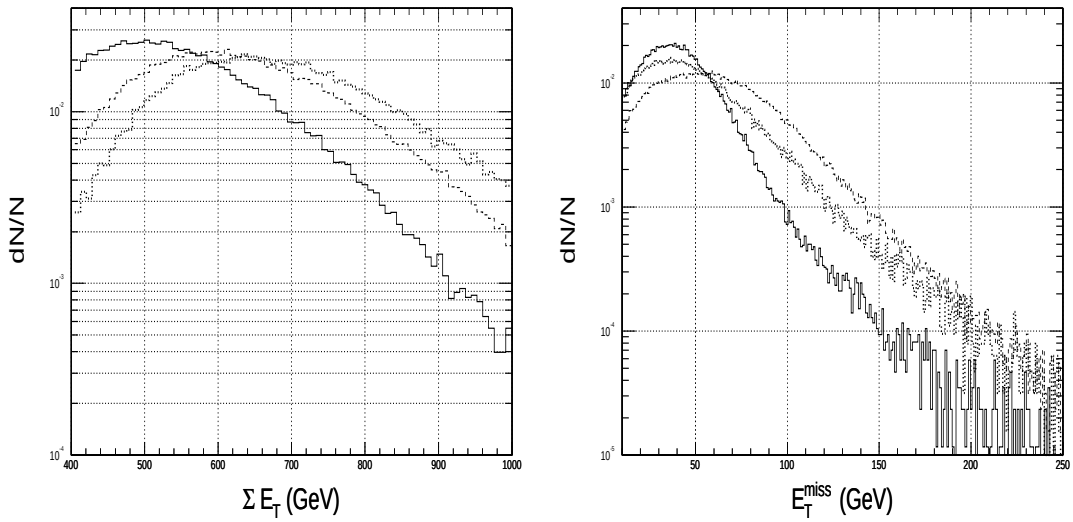

(a) (b)

Figure 19: Reconstructed (a) ΣE_{T} and (b) $E_{\mathrm{T}}^{\mathrm{miss}}$ in $\mathrm{t\bar{t}}$ events (dashed line), $\mathrm{t\bar{t}}$ with a forced W leptonic decay at the generator (dotted line) and W+jet events with W p_T between 40 and 300 GeV (solid line).

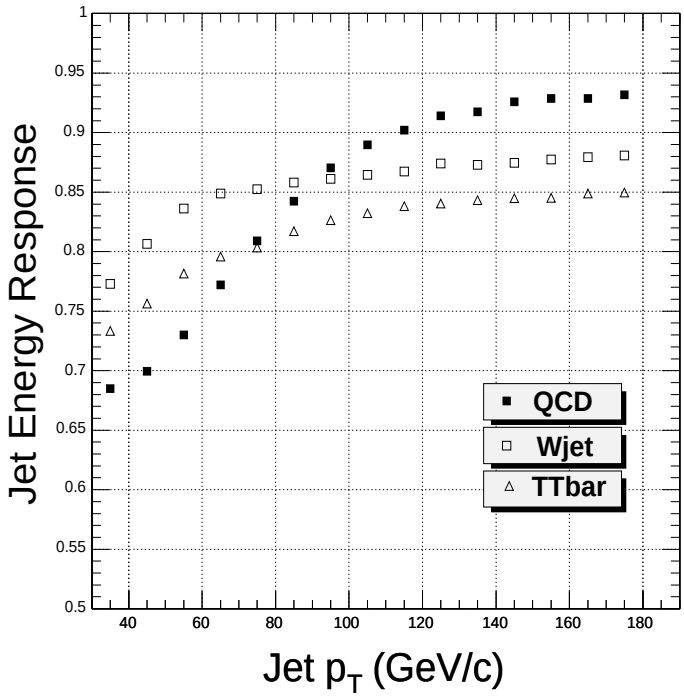

Figure 20: Uncorrected jet response in QCD (solid suares), W+jet (open squares) and $\mathrm{t\bar{t}}$ samples (triangles) *vs.* generated jet p_{T}.

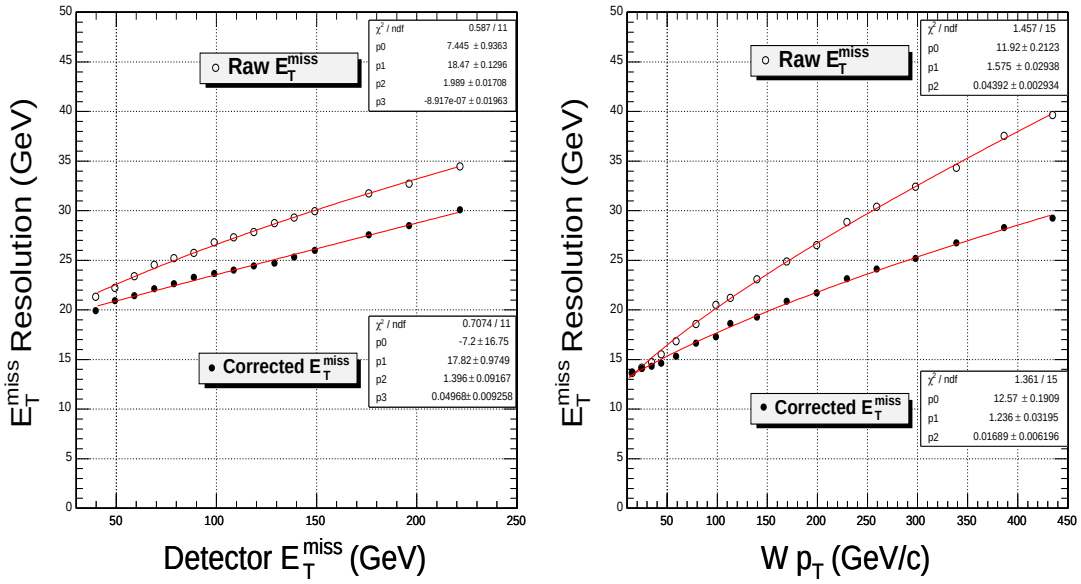

(a) (b)

Figure 21: Missing transverse energy resolution before and after jet corrections for (a) $\mathrm{t\bar{t}}$ events *vs.* reconstructed $E_{\mathrm{T}}^{\mathrm{miss}}$ and (b) W+jet events *vs.* W p_{T}.

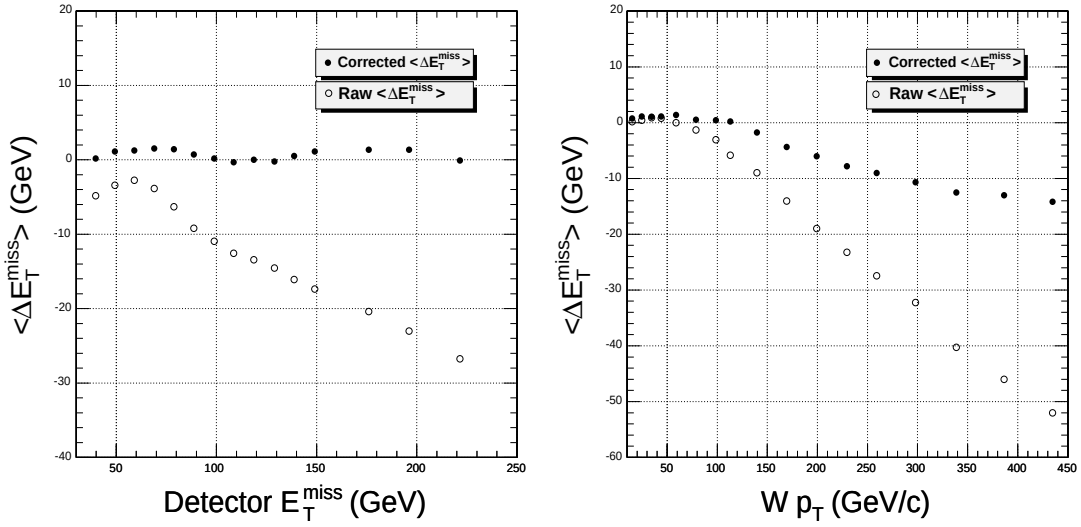

(a) (b)

Figure 22: Error in the reconstructed missing transverse energy scale before and after jet corrections for (a) $\mathrm{t\bar{t}}$ events *vs.* reconstructed $E_{\mathrm{T}}^{\mathrm{miss}}$ and (b) W+jet events *vs.* W p_{T}.

9 Angular Resolution

To establish a signature for missing transverse energy in an event, it is likely necessary to show that the vector $\mathbf{E}_{\mathrm{T}}^{\mathrm{miss}}$ does not have the same φ as an energetic jet whose energy fluctuation in the calorimeter may well have been the cause of the reconstructed $E_{\mathrm{T}}^{\mathrm{miss}}$. Figure 23 shows the $\mathbf{E}_{\mathrm{T}}^{\mathrm{miss}}$ angular resolution as a function of reconstructed $E_{\mathrm{T}}^{\mathrm{miss}}$ in $\mathrm{t\bar{t}}$ events with leptonic decays having $p_{\mathrm{T}}^{\ell} > 20$ GeV before (open circles) and after (closed circles) Monte Carlo corrections to the jet energies. The resolution is calculated by fitting the distribution $\varphi_{\mathrm{r}} - \varphi_{\mathrm{g}}$, where φ_{r} (φ_{g}) is the azimuthal angle of the reconstructed (generated) missing transverse energy vector. The angular resolution for measured $E_{\mathrm{T}}^{\mathrm{miss}} = 45$ GeV is comparable to the jet cone size (0.5 radian) but improves at $E_{\mathrm{T}}^{\mathrm{miss}} = 100$ GeV to the jet core size (0.2 radian) [9]. At larger values of $E_{\mathrm{T}}^{\mathrm{miss}}$, the resolution approaches that of the hadronic tower size (0.1 radian). The Monte Carlo corrections of the missing transverse energy vector make only a small improvement, approximately 0.02 radians for reconstructed $E_{\mathrm{T}}^{\mathrm{miss}} = 100$ GeV, to the angular resolution.

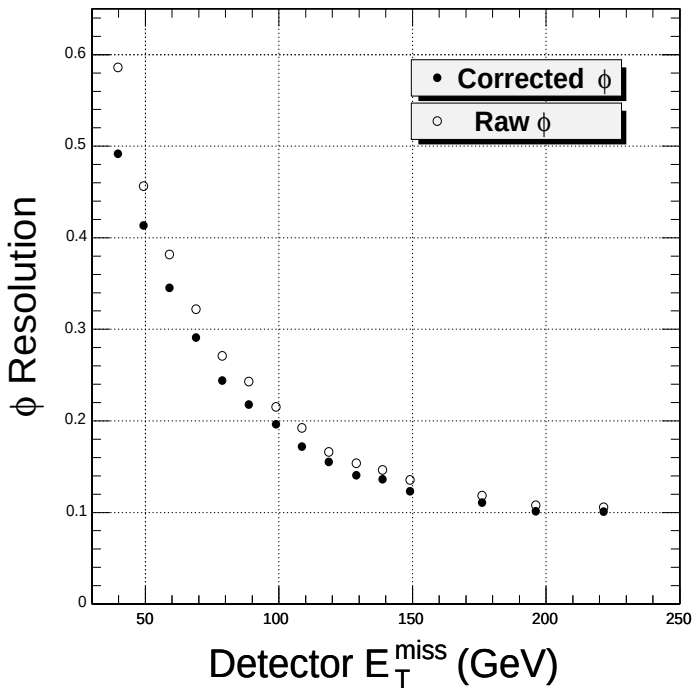

Figure 23: Phi resolution of the vector $\mathbf{E}_{\mathrm{T}}^{\mathrm{miss}}$ as a function of reconstructed $E_{\mathrm{T}}^{\mathrm{miss}}$ in $\mathrm{t\bar{t}}$ events with leptonic decays having $p_{\mathrm{T}}^{\ell} > 20$ GeV before (open circles) and after (closed circles) Monte Carlo corrections to the jet energies.

The missing transverse energy angular resolution has also been studied for W+jet events with leptonic decays having $p_{\mathrm{T}}^{\ell} > 20$ GeV, which have a different topology than $\mathrm{t\bar{t}}$ events. In this case, the missing transverse energy tends to be opposite in φ to an energetic jet whose mismeasurement contributes directly to the reconstructed $E_{\mathrm{T}}^{\mathrm{miss}}$. Figure 24 shows the missing transverse energy φ resolution as a function of reconstructed W transverse momentum. The W p_{T} is approximately twice the average p_{T} of an energetic neutrino which causes a non-zero reconstructed missing transverse energy. Thus, events with W $p_{\mathrm{T}} = 200$ GeV$/c$, which have a missing transverse energy φ resolution of about 0.2 radians, correspond to a 100 GeV neutrino in agreement with Fig. 23.

10 Summary

The missing tranaverse energy performance of the CMS detector has been evaluated using fully simulated minimum bias, QCD, $\mathrm{t\bar{t}}$, and W+jet events with high statistics. For miminum bias events without pileup, a resolution of 6.1 GeV is expected, corresponding to a stochastic contribution of $0.63\sqrt{\Sigma E_{\mathrm{T}}}$ GeV$^{1/2}$, where ΣE_{T} is the summed transverse energy in all calorimeter towers. This result is in agreement with expectatons from measurements at UA1 and CDF, taking into account differences in calorimeter resolution. When the contribution of pileup is included, the resolution degrades according to the overall deposited ΣE_{T} with the same stochastic coefficient. For QCD events, we expect $\sigma = [(3.8\ \mathrm{GeV})^2 + (0.97\ \mathrm{GeV}^{1/2}\sqrt{\Sigma E_{\mathrm{T}}})^2 + (0.012\Sigma E_{\mathrm{T}})^2]^{1/2}$ resulting in a resolution of 45 GeV for jet events with transverse momentum of 700 GeV/c. A sample of $\mathrm{t\bar{t}}$ events with lepton decays

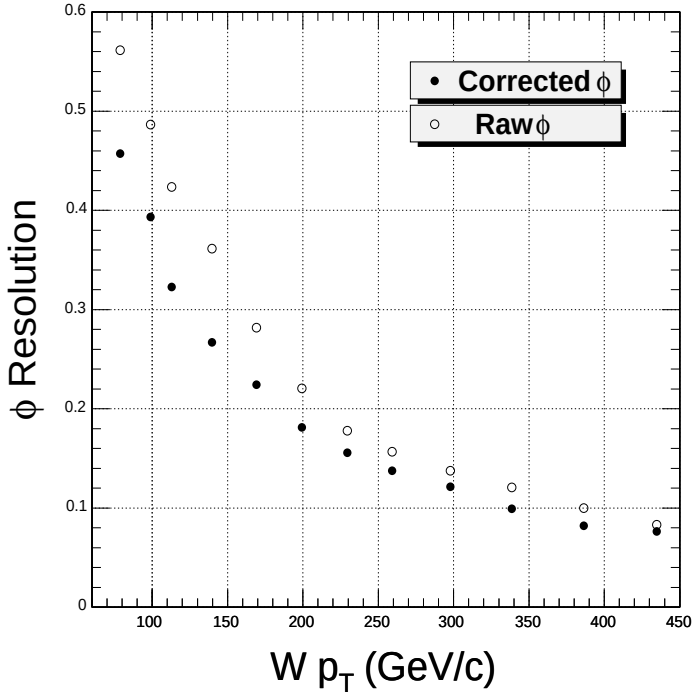

Figure 24: Phi resolution of the vector $\mathbf{E}_{\mathrm{T}}^{\mathrm{miss}}$ as a function of reconstructed W transverse momentum in inclusive W+jet events with leptonic decays having $p_{\mathrm{T}}^{\ell} > 20\,\mathrm{GeV}$ before (open circles) and after (closed circles) Monte Carlo corrections to the jet energies.

leading to true missing transverse energy was used to detemine the azimuthal angle resolution to be 0.1 radians (0.2 radians) for a reconstructed missing transverse energy of 200 GeV (100 GeV).

References

[1] A. Astbury *et al.*, "A 4π Solid-Angle Detector for the SPS Used as a Proton-Antiproton Collider at a Centre-of-Mass Energy of 540 GeV," CERN/SPSC 78-06 (1978).

[2] "CMS, The Hadron Calorimeter Technical Design Report," CERN/LHCC 97-31 CMS TDR 2 (June 1997).

[3] G. Arnison *et al.*, "Experimental Observation of Isolated Large Transverse Energy Electrons With Associated Missing Energy at $\sqrt{s} = 540$ GeV," Phys. Lett. **122B** (1983) 103.

[4] See, for example, G. Arnison *et al.*, "Events With Large Missing Transverse Energy at the CERN Collider: I. $\mathrm{W} \to \tau\nu$ Decay and Test of $\tau - \mu - \mathrm{e}$ Universality at $Q^2 = m_{\mathrm{W}^2}$," Phys. Lett. **185B** (1987) 233; G. Arnison *et al.*, "Events With Large Missing Transverse Energy at the CERN Collider: II. Search for the Decays of $\mathrm{W}^{\pm}$ Into Heavy Leptons and of Z^0 Into Non-Interacting Particles", Phys. Lett. **185B** (1987) 241; G. Arnison *et al.*, "Events With Large Missing Transverse Energy at the CERN Collider: III. Mass Limits on Supersymmetric Particles," Phys. Lett. **198B** (1987) 261.

[5] F. Abe *et al.*, "Search for Gluinos and Squarks at the Fermilab Tevatron Collider," Phys. Rev. **D56** (1997) 1357.

[6] "CMS, The Electromagnetic Calorimeter Technical Design Report," CERN/LHCC 97-33, CMS TDR 4 (1997), Addendum CERN/LHCC 2002-27 (2002).

[7] G. Alverson, G. Eulisse, S. Muzaffar, I. Osborne, L. Taylor, and L. A. Tuura, "IGUANA: A high-performance 2D and 3D visualisation system," Nucl. Instrum. and Meth. **A534** (2004) 143.

[8] C. Albarjar *et al.*, "Analysis of the Highest Transverse Energy Events Seen in the UA1 Detector at the Sp$\bar{\mathrm{p}}$S Collider," Z. Phys. **C36** (1987) 33.

[9] G. Arnison *et al.*, "Hadronic Jet Production at the Cern Proton-Antiproton Collider," Phys. Lett. **132B** (1983) 214.

[10] F. Abe *et al.*, "Measurement of the W-boson Mass," Phys. Rev. Lett. **65** (1990) 2243.

[11] CMS HCAL Collaboration, "Design, Performance, and Calibration of CMS Hadron-Endcap Calorimeter Wedges," submitted to Nucl. Inst. and Meth.

[12] CMS, The TriDAS Project, Technical Design Report, Volume 2: Data Acquisition and High-Level Trigger, CERN/LHCC 2002-26, CMS TDR 6.2 (2002).

[13] CMS Collaboration, "The Computing Project Technical Design Report," CERN/LHCC 2005-23 (2005), CMS TDR 7.

[14] T. Sjstrand, P. Edn, C. Friberg, L. Lnnblad, G. Miu, S. Mrenna and E. Norrbin, "High-Energy-Physics Event Generation with PYTHIA 6.1," Computer Phys. Commun. 135 (2001) 238 (LU TP 00-30, hep-ph/0010017).

[15] V. Karimki, "CMKIN, CMS Physics Generators Interface," http://cmsdoc.cern.ch/cmsoo/projects/CMKIN/.

[16] GEANT4 Collaboration, S. Agostinelli *et al.*, "GEANT4: A Simulation Toolkit," Nucl. Instr. and Meth. **A506** (2003) 250.

[17] M. Stavrianakou, "OSCAR: Object-oriented Simulation for CMS Analysis and Reconstruction," http://cmsdoc.cern.ch/OSCAR/.

[18] S. Wynhoff, "ORCA: CMS Object-Oriented Reconstruction," http://cmsdoc.cern.ch/orca/.

[19] H. Pi, "CMS JetMET Datasets in DC04 and Post-DC04," http://cms00.phys.ufl.edu/cms/DC04/PCP/.

[20] O. Kodolova *et al.*, "Jet Energy Correction with Charged Particle Tracks in CMS," "Eur. Phys. J. **C40S2** (2005) 33.

[21] ATLAS Collaboration, "ATLAS Detector and Physics Performance Technical Design Report," CERN/LHCC 99-14 (1999) ATLAS TDR 14.

[22] "Measurement of Jets With the CMS Detector at the LHC," CMS Note 2005-xxx.

[23] A. Nikitenko, S. Kunori, and R. Kinnunen, "Missing Transverse Energy Measurement with Jet Energy Corrections," CMS NOTE 2001/040 (2001).